

Chapter 10

Superhydrophobic and Water-Repellent Polymer-Nanoparticle Composite Films

Ioannis Karapanagiotis and Panagiotis Manoudis

Abstract The wetting properties of the surfaces of polymer films changed dramatically from the usual inherent hydrophobicity (or slight hydrophilicity) to superhydrophobicity (contact angle, $CA > 150^\circ$) by embedding oxide nanoparticles into the polymer matrices. The desired hierarchical roughness at the micrometer and nanometer scale was induced in poly(methyl methacrylate), polystyrene, and four poly(alkyl siloxane) films enriched with silica, tin oxide, alumina, and zinc oxide nanoparticles, ranging from 7 to 70 nm in mean diameter. Particles were added in the polymer solutions which were afterward sprayed on various substrates, such as glass, silicon, concrete, aluminum, silk, paper, wood, marble (white), sandstone, and mortar. It is stressed that superhydrophobicity was accompanied by water repellency, as evidenced by the low contact angle hysteresis ($CAH < 10^\circ$). Consequently, it is demonstrated that the simple suggested method for transforming the wetting properties of polymer films to achieve extreme nonwetting is flexible as it can be effectively applied using different materials, including polymers and nanoparticles of low cost. Moreover, the method can be easily used for the surface treatment of large and various substrates. The effects of the (1) concentration and size of the nanoparticles, (2) chemical nature of the polymer matrix, and (3) treated substrate on the wetting properties of the films were investigated and interpreted using scanning electron microscopy (SEM). Finally, it is shown that depending on the color of the underlying substrate, the superhydrophobic water-repellent polymer-nanoparticle films may have a negligible effect on the aesthetic appearance of the treated substrate.

Keywords Superhydrophobic • Water repellent • Polymer nanoparticle • Lotus

I. Karapanagiotis (✉) • P. Manoudis

Department of Management and Conservation of Ecclesiastical Cultural Heritage Objects,
University Ecclesiastical Academy of Thessaloniki, Thessaloniki 54250, Greece
e-mail: y.karapanagiotis@aeath.gr; pan.manoudis@gmail.com

10.1 Introduction

Nanoparticles and nanofillers are often embedded into polymer matrices to produce nanocomposites with improved mechanical, thermal, electronic, or optical properties [1, 2]. With the increased interest on superhydrophobic and water-repellent surfaces, the wetting properties of the surfaces of these nanocomposites have recently attracted considerable attention [3–29]. Nanoparticles, used as additives, can modify the surface structure enhancing, for instance, surface roughness. The latter is a key parameter to achieve superhydrophobicity and water repellency, which was first displayed on hierarchical structured biosurfaces.

Two biological surfaces that have been extensively used as model surfaces to fabricate biomimetics materials of special and controlled wettabilities are that of the lotus leaf and rose petal [30, 31]. Both plant surfaces exhibit superhydrophobic properties, implying that the static contact angle (CA) of a resting water droplet is large, $CA > 150^\circ$. However, the two plant surfaces show different dynamic wetting which is directly related to water repellency/adhesion. That is, water droplets can effortlessly roll off the surface of a lotus leaf (“lotus effect”) [30] whereas they stay pinned to the surface of a red rose petal (“petal effect”) [31], thus corresponding to low and high contact angle hysteresis (CAH), respectively. Hence, industrial materials with lotus leaf-like surfaces are useful for applications relevant to water repellency, self-cleaning, and friction reduction. Artificial surfaces with rose petal properties show water adhesion and therefore have potential for applications such as the controlled transport of small volumes of liquid in open microfluidic devices [32]. Potential applications of biomimetics materials with special wetting properties are discussed at the end of the article.

Several parameters of a binary polymer-nanoparticle film may affect its surface wettability: the roles of the (1) concentration and size of the nanoparticles, (2) polymer matrices, and (3) substrates, used to support the composite films, are investigated herein. Oxide nanoparticles, with sizes ranging from 7 to 70 nm, are dispersed in polymer solutions at various concentrations. Dispersions are afterward sprayed on several substrates, and the wettabilities of the resulting composite polymer-nanoparticle films are investigated with contact angle measurements (CA and CAH) of water drops and interpreted using scanning electron microscopy (SEM). It is shown that the deposited films can have superhydrophobic and water-repellent properties, provided that the key parameters described above have been selected appropriately. Consequently, the studied method can be used to tune the wetting properties of polymer-nanoparticle films and achieve nonwetting.

The method has some important advantages: (1) it is an easy, one-step method; (2) it is of low cost, as it does not include the use of any sophisticated instrumentation or expensive materials; (3) the method can be easily used for the surface treatment of large and various substrates; and finally (4), superhydrophobicity and water repellency are achieved using various oxide nanoparticles and polymers, thus providing a lot of flexibility to engineers who would like to adapt the method using materials, polymers, and nanoparticles according to their needs.

On the other side, a drawback of the suggested method is that it may have an impact on the aesthetic appearance of the treated substrates because the oxide particles are white and therefore not transparent in visible light. As coloring alterations induced by protective coatings are usually undesirable, colorimetric measurements were carried out and discussed in detail.

10.2 Experimental

For most studies described in the following, Rhodorsil was used, which is a poly(methyl siloxane) dissolved in white spirit (mixture of aliphatic and alicyclic hydrocarbons) at a concentration of 7 % wt. Silica nanoparticles, 14 nm in mean diameter, were dispersed in the Rhodorsil solution in various concentrations. The Rhodorsil-silica dispersions were stirred mechanically and sprayed on silicon wafers, used as substrates to support the Rhodorsil-silica nanocomposites. The surfaces of the produced composite films were used for extensive studies. However, other nanoparticles, polymers and substrates, summarized in Table 10.1, were included for further investigations.

Dispersions were applied using an airbrush system with a nozzle of 733 μm in diameter. After drying, the wettabilities of the surfaces of the films were investigated by the sessile drop method using a Krüss DSA 100 apparatus and distilled water. Water droplets were carefully placed on the surfaces and the images of the

Table 10.1 Materials used in the study

Nanoparticle			Polymer solution		Substrate
Material	Mean particle size (nm)	Mean particle SSA (m^2/g)	Polymer	Solvent	
Silica (SiO_2)	7	390	Rhodorsil, poly(methyl siloxane)	White spirit	Glass, silicon, concrete, aluminum, silk, paper, wood, marble (white), sandstone, mortar
Silica (SiO_2)	14	200	PMMA, poly(methyl methacrylate)	Toluene	
Tin oxide (SnO_2)	32.5	30	PS, polystyrene	Toluene	
Alumina (Al_2O_3)	45	36	Silres BS 290, poly(alkyl siloxane)	White spirit	
Zinc oxide (ZnO)	70	17.5	Porosil VV plus, poly(alkyl siloxane)	White spirit	
			Silres BS 4004, poly(alkyl siloxane)	Water	

Nanoparticles of different sizes and specific surface areas (SSAs) were dispersed in various polymer solutions. Dispersions were sprayed on various substrates, described in the table. It is noteworthy that a water-soluble resin (Silres BS 4004) was included in the study

Table 10.2 CA of water droplets on smooth polymer surfaces, which were prepared by spin coating onto silicon wafers

Polymer	CA (°)
PMMA	72
PS	90
Silres BS 290	97
Rhodorsil	102
Porosil	104
Silres BS 4004	111

droplets were captured immediately to measure the static contact angle (CA). The contact angle hysteresis (CAH) was calculated by the dynamic sessile drop method. The advancing/receding contact angle was the maximum/minimum angle measured, while the volume of the droplet was increased/decreased without increasing/decreasing the solid-liquid interfacial area. The reported CA and CAH are averages of several measurements which varied within $\pm 2^\circ$.

The morphologies of the film surfaces were investigated using scanning electron microscopy (SEM, Jeol JSM-840A). Colorimetric measurements were carried out with a MiniScan EZ (HunterLab) instrument, and the results were evaluated using the $L^* a^* b^*$ coordinates of the CIE 1976 scale. L^* , a^* , and b^* are the brightness (0 for black and 100 for white), the red-green component (positive for red and negative for green), and the yellow-blue component (positive for yellow and negative for blue), respectively.

Finally, solutions of pure polymers (without particles) were spin coated onto silicon wafers to produce smooth surfaces and to evaluate the inherent degree of hydrophobicity of the organic materials. CA measurements of water droplets on these very smooth polymer surfaces are summarized in Table 10.2.

10.3 Results and Discussion

10.3.1 *Effect of the Particle Concentration on the Wettability of the Composite Films*

Figure 10.1a shows the variations of the static contact angle (CA) and the contact angle hysteresis (CAH) with particle concentration, for water droplets placed on Rhodorsil-silica (14 nm) films. The CA initially increases with particle concentration from 105° , for pure Rhodorsil without particles, to 163° for 1 % w/v or higher particle concentrations. Further increase in particle concentration (>1 % w/v) does not have any significant effect on the CA which is (1) stable, corresponding to the plateau of the curve in Fig. 10.1a, and (2) extremely high, ($>150^\circ$) corresponding to superhydrophobicity. As silica is a hydrophilic material, it is safe to conclude that the nanoparticles only contribute to surface roughness, while it is the siloxane polymer that is in the topmost layer all over the surface [6, 21, 33].

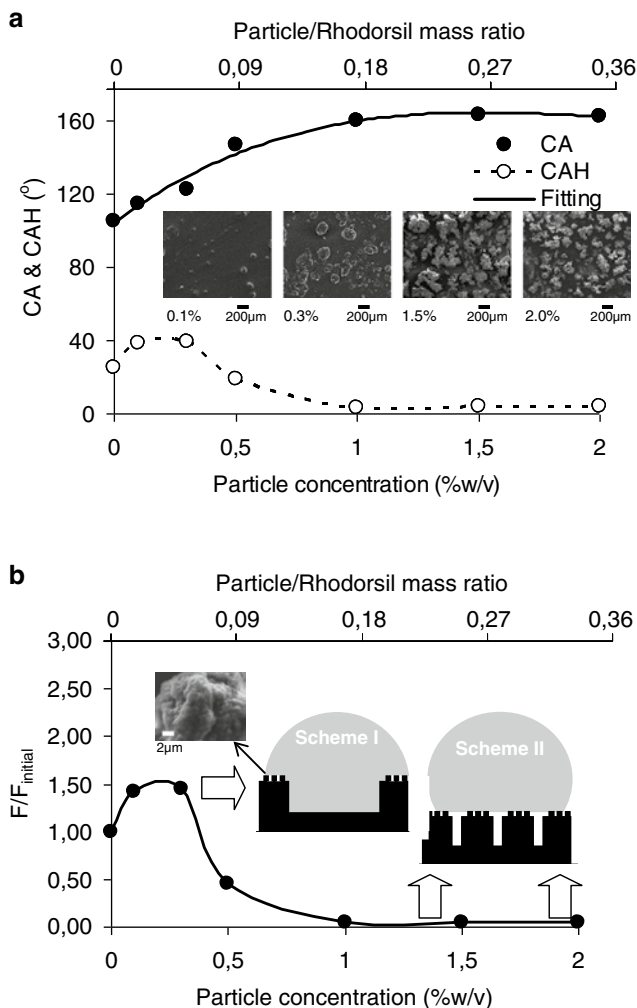


Fig. 10.1 (a) Static contact angle (CA) and contact angle hysteresis (CAH) versus the concentration of silica particles (14 nm) embedded in Rhodorsil. Films were deposited on silicon wafers. The data of CA is fitted with a three-order polynomial function to guide the eye. SEM images revealing the evolution of surface structure are included. (b) Force needed to start a drop moving over the Rhodorsil-silica film surface (F) normalized to its initial value ($F_{initial}$), which corresponds to pure Rhodorsil, versus the particle concentration. Schemes I and II show the wetting scenarios for films prepared using low and high particle concentration, respectively. The nanorecives existing on the protruded clusters are revealed by the SEM image

The results of the CA in Fig. 10.1a are in agreement with previously published studies which described the effect of nanoparticles on the surface of polymer-nanoparticle composite films [6, 13, 19, 21]. Nanoparticles form microscale clusters which enhance the roughness of the surface at the micrometer/nanometer scale. Initially, the clusters are randomly distributed and are separated by smooth areas of continuous polymer film, as shown in the SEM images of Fig. 10.1a, captured for films prepared using dispersions of 0.1 and 0.3 % w/v nanoparticles. Larger (coalesced) clusters are formed at elevated particle concentrations, resulting in a continuous rough surface according to the SEM images corresponding to 1.5 and 2 % w/v particle concentration. This dense rough surface structure is responsible for the observed superhydrophobicity, as it was first evidenced on the surfaces of various plants, including that of the lotus leaf [30].

The variation of the CAH with particle concentration is more complicated compared to the behavior of CA, described above. According to the results of Fig. 10.1a, as the particle concentration increases, an increase in CAH is first recorded, which reaches a maximum value and then decreases. At the particle concentration of around 1 % w/v, CAH is minimized ($<5^\circ$) and becomes constant. The variation of CAH with particle concentration is interpreted by the SEM images included in the same Fig. 10.1a. Water may fill the large, smooth interspaces that exist, among the clusters, in films prepared using low particle concentration. Therefore, the clusters may act as pinning sites resulting in an increase of CAH. As the particle concentration increases, a continuous rough structure is formed eliminating the pinning sites, thus decreasing droplet adhesion and enhancing repellency. Therefore this change of the surface morphology is accompanied by a drop of CAH which reaches a very small value. As the surface structure of the Rhodorsil-silica film becomes saturated, both CA and CAH become constant, corresponding to very high and low values, respectively. Consequently, both superhydrophobicity and water repellency occur at the surfaces of the films which correspond to particle concentration >1 % w/v.

According to the SEM images of Fig. 10.1a, surface roughness increases with particle concentration. This was observed in previous studies on polymer-nanoparticle composites [6, 7, 13, 14, 19, 21]. Consequently, it can be argued that the horizontal axis of the plot in Fig. 10.1a corresponds qualitatively to surface roughness. Therefore, it is concluded that the variation of CAH in Fig. 10.1a is in agreement with the results reported by (1) Johnson and Dettre who measured the advancing and receding contact angles of water drops on wax [34], (2) Tserepi et al. who carried out CAH measurements on plasma-treated PDMS surfaces [35], and (3) Morra et al. who reported advancing and receding contact angles on plasma-treated PTFE surfaces [36]. Finally, the CAH variation reported in Fig. 10.1a for composites prepared using 14 nm silica particles is in excellent agreement with a previous investigation where the effect of 7 nm silica nanoparticles on the wettability of a siloxane-silica composite was reported [6].

As described previously, superhydrophobicity is assessed by the large CA. However, water repellency or adhesion is evaluated through CAH, which is directly related to the force needed to start a drop moving over a solid surface [37]:

$$F = \gamma_{lv} (\cos RCA - \cos ACA) \quad (10.1)$$

where F is the critical force per unit length, γ_{lv} the liquid-vapor interfacial surface tension, and RCA and ACA are the receding and advancing contact angles, respectively. According to Eq. (10.1), F must vary according to CAH which is the difference between ACA and RCA ($CAH = ACA - RCA$). This is shown in the plot of Fig. 10.1b where the force F normalized to its initial value, $F_{initial}$, is shown as a function of the particle concentration. The curve in Fig. 10.1b follows the behavior of CAH reported in Fig. 10.1a. Two schemes illustrating water droplets on the rough surfaces are provided. As argued previously, in scheme I (low particle concentration), water fills the large, smooth areas that exist among the clusters. In this case, clusters act as pinning sites resulting in an increase of F . However, it is quite possible that water does not penetrate the nanorecives (SEM image in Fig. 10.1b) that exist on the surface of the protruding clusters because of the Laplace pressure. Apparently, scheme I cannot be rationalized by the Cassie-Baxter model [38] which can be applied to interpret the scenario of scheme II (high particle concentration), where a dense rough structure exists inducing non-sticking properties. In the Cassie-Baxter state of scheme II, the force F is extremely small, as evidenced by the results of Fig. 10.1b. In particular, for particle concentration ≥ 1 % w/v, $F/F_{initial}$ equals 0.05, implying that it takes 20 times as less force to move a drop on Rhodorsil-silica than on a pure Rhodorsil film. On the contrary, a higher F than $F_{initial}$ must be applied when the scenario of scheme I is realized.

10.3.2 *Effect of the Particle Size on the Wettability of the Composite Films*

Figure 10.2 shows the CA and CAH measurements of water droplets on Rhodorsil-nanoparticle composites which were prepared using five different nanoparticles: silica (of two sizes), tin oxide, alumina, and zinc oxide. The particles are described in Table 10.1. For comparison, the CA and CAH measured on pure Rhodorsil (without nanoparticles) are included in the graph. It is stressed that the Rhodorsil-silica composites were prepared using 2 % w/v particle concentration. Higher concentrations (10 % w/v) of tin oxide, alumina, and zinc oxide nanoparticles were embedded in the Rhodorsil matrix to achieve the results reported in Fig. 10.2. The cross-influence effect of particle size and concentration on the wettability of the composite film is discussed later. The goal of Fig. 10.2 is to prove that superhydrophobicity ($CA > 150^\circ$) and water repellency ($CAH < 10^\circ$) can be achieved using various nanoparticles ranging from a few, up to several tenths of nanometers. This result is important because it provides the flexibility to select appropriate nanoparticles depending on the desired application. Karapanagiotis et al. [39] and Ogihara et al. [16] showed that superhydrophobicity can be induced using nanoparticles that are up to 150 and 200 nm in mean diameter, respectively (i.e., particles bigger

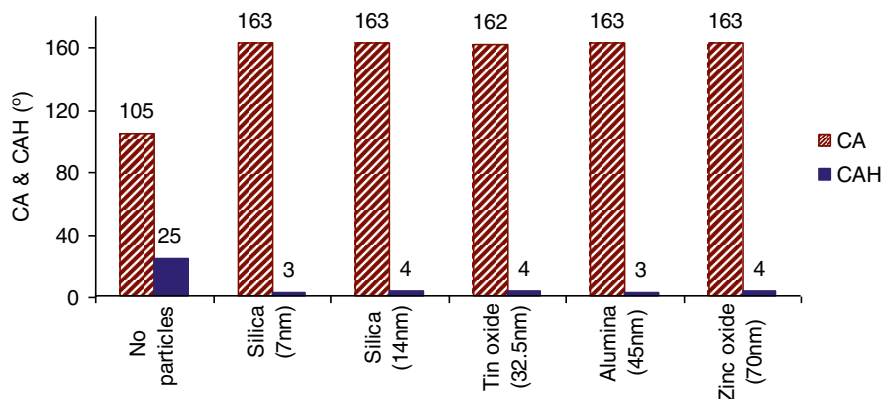


Fig. 10.2 CA and CAH on Rhodorsil-nanoparticle composites which were prepared using the particles of Table 10.1. Particle concentrations used to prepare the films were as follows: 2 % w/v silica (of two sizes) and 10 % w/v tin oxide, alumina, and zinc oxide. For comparison, CA and CAH on pure Rhodorsil (no particles) are included. CA and CAH are independent of the particle used; as for the five composite films, the angles range within only 162–163° and 3–4°, respectively. Consequently, the wettabilities of the five composite films are similar and clearly different than the hydrophobic character of the pure Rhodorsil (no particles) which is described by a low CA (105°) and high CAH (25°)

than the 70 nm zinc oxide particles included in Fig. 10.2). Ogiwara et al. [16] indicated that superhydrophobicity is not achieved when particles of 500 nm in mean diameter (or higher) are embedded in the polymer matrix. Consequently, the high CA values reported in Fig. 10.2 are in agreement with the two previously published reports [16, 39]. Furthermore, Fig. 10.2 shows that the superhydrophobic and water-repellent characteristics of the composite films are not affected by the size and chemical nature of the nanoparticles. For the five nanoparticles included in Fig. 10.2, CA varies only between 162 and 163°, whereas CAH falls within 3–4°. Consequently, the wetting properties of the five composite films are similar. This result offers support to the argument provided previously that nanoparticles only contribute to surface roughness, while it is the polymer that is in the topmost layer all over the surface.

Figure 10.3 shows the variation of CA with particle concentration for Rhodorsil-silica (7 nm) and Rhodorsil-zinc oxide films, which are the composites prepared using the smallest and biggest nanoparticles of the study (Table 10.1). The two curves in Fig. 10.3 follow the tendency explained in Fig. 10.1a. In both sets of data of Fig. 10.3, the same maximum CA is achieved (163°) corresponding to the plateaus of the two curves. This maximum CA was reported in Fig. 10.2 and it is independent of the particle size. However, Fig. 10.3 clearly shows that in order to achieve the maximum CA, different particle concentrations must be used for nanoparticles of different sizes. More/less nanoparticles must be embedded in the polymer matrix when big/small nanoparticles are used to achieve the maximum superhydrophobicity.

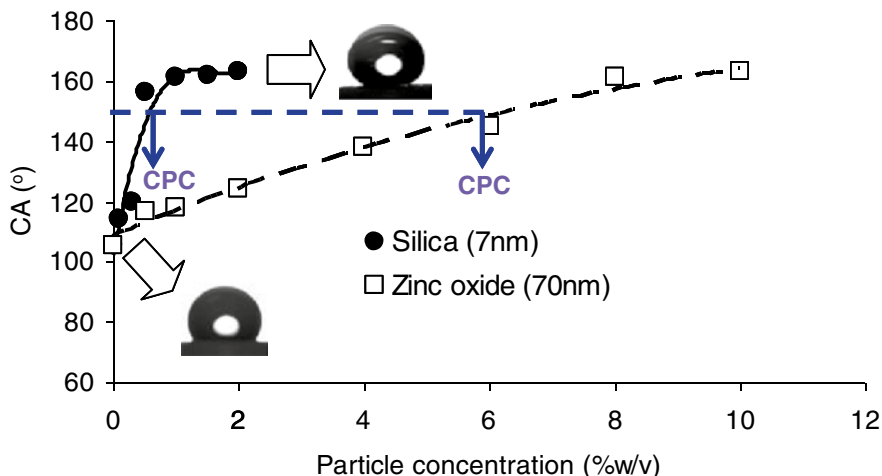


Fig. 10.3 CA versus the concentration of silica (7 nm) and zinc oxide (70 nm) particles embedded in Rhodorsil. The two sets of data are fitted with three-order polynomial functions. Photographs of water drops on hydrophobic, pure Rhodorsil and superhydrophobic composite films are included. The calculation of the critical particle concentrations (CPCs) corresponding to $CA = 150^\circ$ is illustrated for the two curves

Figure 10.4 provides a better understanding of the cross-influence effects of particle size and concentration on the wettability of the composite films. The vertical axis of the plot corresponds to the critical particle concentration (CPC), defined as the minimum particle concentration that must be used to achieve superhydrophobicity [39], that is, the particle concentration which corresponds to $CA = 150^\circ$. CPCs corresponding to the Rhodorsil-silica (7 nm) and Rhodorsil-zinc oxide composite films were illustrated in Fig. 10.3. The horizontal axis of the plot in Fig. 10.4 corresponds to the particle specific surface area (SSA) and not to the particle size. SSA values for the five nanoparticles included in the study are given in Table 10.1. The SSA is the fundamental property of the particles which is responsible for the creation of the “new surface” and the increase of surface roughness, occurring with the addition of the particles into the polymer matrix. Because surface roughness directly affects the wetting properties of a surface, it is concluded that SSA must be included in the study’s considerations. In principle, SSA is related to the particle size; the smaller the particle, the higher the SSA. However, this rough rule is not always correct, as evidenced by the data of tin oxide and alumina particles in Table 10.1. Consequently, the variation of CPC for different composites should be studied with respect to the SSA and not to the actual particle size. For this reason SSA is used in the plot of Fig. 10.4.

Figure 10.4 shows that when particles of high SSA are used for the preparation of the polymer-particle composite, low CPC is required to achieve superhydrophobicity. Two regimes are defined in Fig. 10.4: (1) a superhydrophobic regime that falls above the CPC curve and (2) a hydrophobic regime that falls below the fit of the data. The tendency of the curve shown in Fig. 10.4 is similar to the behavior reported

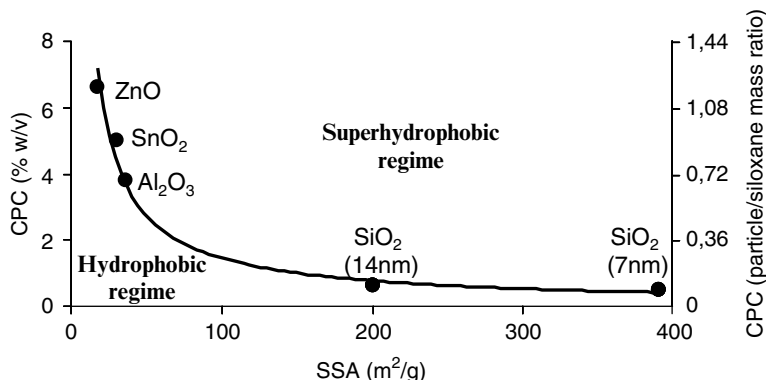


Fig. 10.4 Critical particle concentration (CPC) corresponding to $CA=150^\circ$ versus the particle specific surface area (SSA). The results are fitted with a smooth *line*, which reveals the tendency of the data and is useful to guide the eye

previously for polymer-nanoparticle composite films which were prepared using three alumina nanoparticles of different sizes [39]. Furthermore, the plot of Fig. 10.4 shows that decreasing the SSA from 390 to 200 m²/g does not have any significant effect on the CPC and that the two silica nanoparticles used herein had comparable effects on the wettability of the composite films. However, decreasing the SSA from 200 to 36 m²/g (SSA of the alumina particle) results in a considerable increase of the measured CPC which becomes very sensitive to any further decrease of the SSA.

10.3.3 *Effect of the Polymer on the Wettability of the Composite Films*

In the last section, the same polymer (Rhodorsil) was blended with different nanoparticles. Here, the same type of particles, that is, silica (7 nm), at a concentration of 2 % w/v, is dispersed in solutions of six polymers including PMMA, PS, Silres BS 290, Porosil, Silres 4004, and Rhodorsil. Solvents used to prepare the solutions are described in Table 10.1. According to Table 10.2, CAs measured on smooth surfaces of the aforementioned polymers range from 72 to 111°. Consequently, the inherent wetting properties of the tested polymers are very different.

Figure 10.5 shows the CA and CAH results, obtained for the polymer-silica composites which were prepared using the six polymers. It can be seen that superhydrophobicity ($CA > 150^\circ$) and water repellency ($CAH < 10^\circ$) were achieved on any of the tested polymer-silica surfaces. Interestingly, a considerable variation is observed on the reported CAs ranging from 153° (PMMA-silica) to 166° (Silres 4004-silica). The origin of this variation is discussed next.

The wettabilities of the six surfaces included in Fig. 10.5 correspond to the non-sticking, Cassie-Baxter state. The Cassie-Baxter equation correlates the elevated

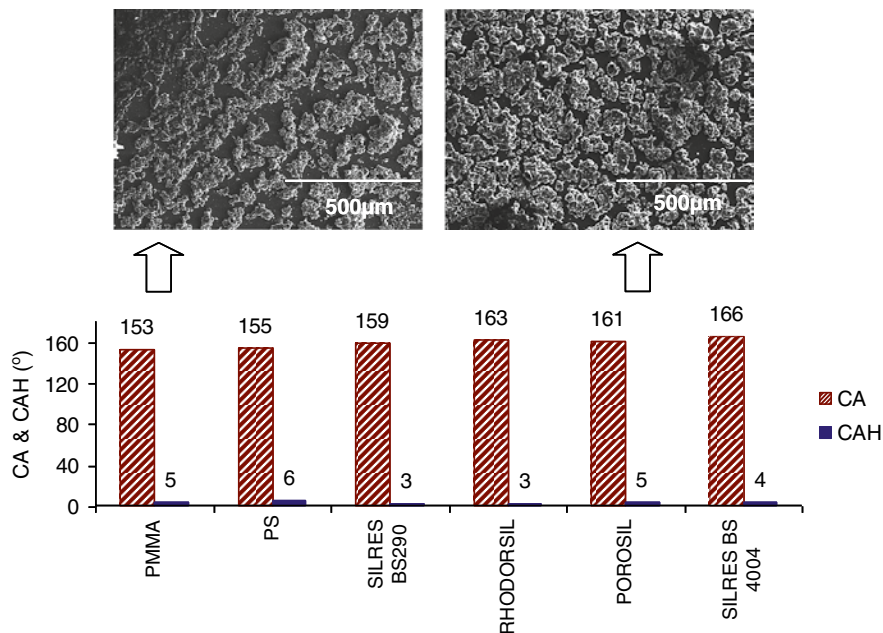


Fig. 10.5 CA and CAH on polymer-silica composites which were prepared using 2 % w/v silica nanoparticles (7 nm) and six different polymers which are labeled in the horizontal axis of the plot. SEM images revealing the surfaces of PMMA-silica and Porosil-silica films are included

apparent contact angle (θ^*) observed on a surface with augmented roughness and the contact angle (θ) measured on a smooth surface [38]:

$$\cos\theta^* = -1 + f_s (\cos\theta + 1) \quad (10.2)$$

where f_s is the surface porosity factor, that is, the fraction of the rough surface which is in direct contact with water. The f_s factors of the six superhydrophobic composite films included in Fig. 10.5 can be calculated, using Eq. (10.2). The angles θ and θ^* correspond to the CAs on pure (smooth) polymers and on composite (rough) films, respectively. The former (θ) are provided in Table 10.2 and the latter (θ^*) are shown in Fig. 10.5. It is reported that the calculated f_s factors varied within a very narrow range, from 0.05 to 0.09, thus implying that the surfaces of the six composite films should exhibit similar structures. Indeed, the SEM images of the PMMA-silica and Porosil-silica films, shown in Fig. 10.5, look very similar.

Because the surface structures of the six composite films are similar, it can be argued that the variation in the CAs of the composite films (Fig. 10.5) originated exclusively from the different chemical natures of the polymers used to prepare the composites. This argument is supported by the results of Fig. 10.6, which shows the plot of the CAs of the rough (superhydrophobic) composites versus the CAs of the smooth, pure polymers. Angles are plotted in terms of their cosines. It is shown that a

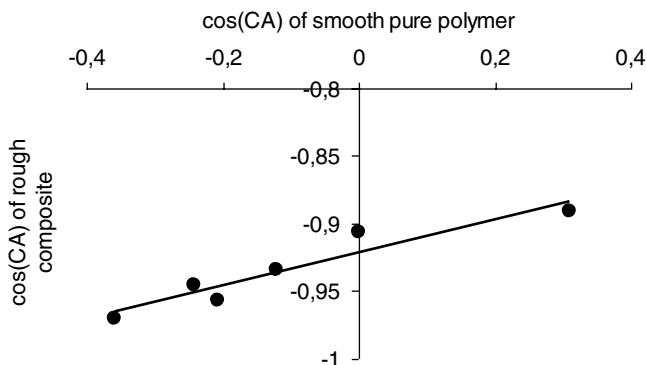


Fig. 10.6 CA on rough polymer-silica (superhydrophobic) composites versus CA on smooth, pure polymer. Angles are plotted in terms of their cosines. A linear function is used to fit the data

linear function provides a good fit for the results, thus implying that the application of the Cassie-Baxter equation (Eq. 10.2) using a single value for f_s is possible to describe the wettabilities of the six different composites. Consequently, the variation of the CAs of the six superhydrophobic composite films reported in Fig. 10.5 originated from the variation of the CAs of the pure polymers (Table 10.2), that is, the different chemical characteristics of the pure polymers. Using the linear fit of the data in Fig. 10.6, it can be calculated that θ^* obtains the critical value of 150° when $\theta = 63^\circ$. Consequently, superhydrophobicity can be achieved in a composite polymer-silica film only if the contact angle of the smooth polymer used is equal or higher than 63° .

10.3.4 Effect of the Underlying Substrate on the Wettability of the Composite Films

Figure 10.7 shows CA and CAH measurements of water droplets on Rhodorsil-silica (7 nm and 2 % w/v) composites which were deposited on various substrates. It is seen that superhydrophobicity ($CA > 150^\circ$) and water repellency ($CAH < 10^\circ$) were achieved on any of the tested surfaces. This result shows that the spray method can be used to induce nonwetting properties to various inherently hydrophilic materials, by applying polymer-nanoparticle films. This is an important finding as it enhances the versatility of the suggested method which can be easily applied to treat large and different surfaces. Films included in Fig. 10.7 were prepared using 2 % w/v silica (7 nm) nanoparticles and Rhodorsil. At this relatively high level of particle concentration, the surface structure is extremely rough, inducing wetting properties which are practically unaffected by the underlying substrate. Both CA and CAH reported in Fig. 10.7 for various treated substrates show narrow ranges of variations.

Figure 10.8 shows the variation of CA with particle concentration for Rhodorsil-silica (7 nm) films deposited on glass and sandstone. The two substrates exhibit different surface morphologies, as glass is atomically smooth whereas sandstone is

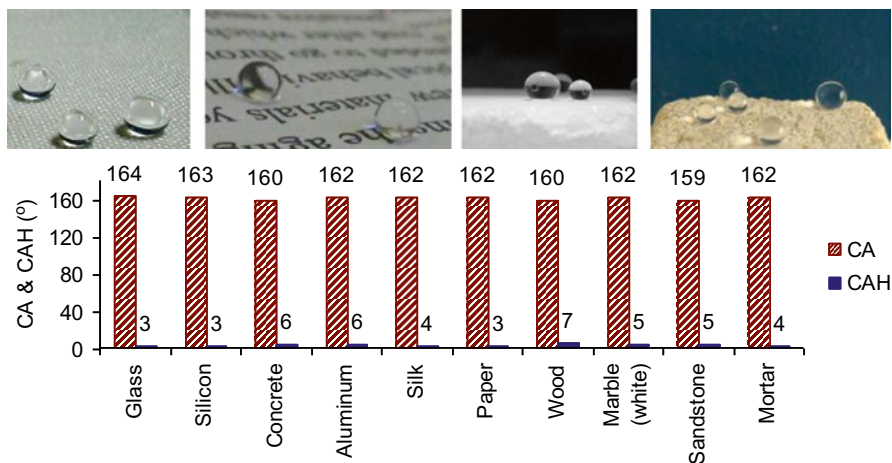


Fig. 10.7 CA and CAH on Rhodorsil-silica composites which were prepared using 2 % w/v silica nanoparticles (7 nm). Composite films were deposited on different substrates as indicated in the horizontal axis of the plot. Photographs showing water drops on silk, paper, marble, and sandstone are included

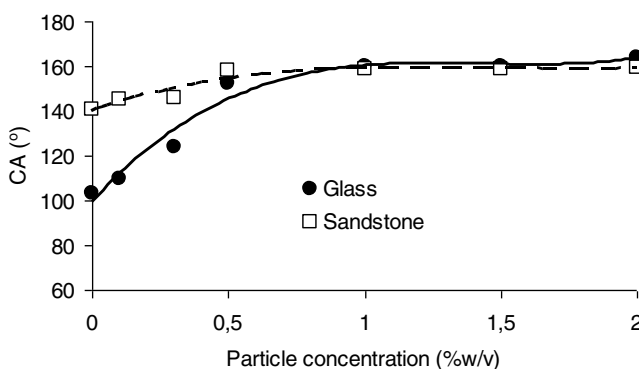


Fig. 10.8 CA versus the concentration of silica nanoparticles (7 nm) embedded in Rhodorsil. The composite films were deposited on glass and sandstone. The two sets of data are fitted with three-order polynomial functions to guide the eye

rough, corresponding to a surface porosity on the order of 8 % [10]. This difference between glass and sandstone does not affect the maximum CA obtained in Fig. 10.8 for the two sets of data. The maximum CA is achieved using high particle concentration (≥ 1 % w/v) and is practically unaffected by the underlying substrate. This result is in agreement with the CA measurements presented in Fig. 10.7, which corresponds to a 2 % w/v particle concentration.

However, according to Fig. 10.8, the role of the substrate roughness becomes important for films prepared using low particle concentration (< 1 % w/v). The CA for a smooth Rhodorsil film (no particles) on glass is only 103°. However, the

Rhodorsil film on sandstone exhibits a roughness which originated from the roughness of the underlying substrate. Consequently, the CA measured on pure Rhodorsil (no particles) deposited on sandstone is 141° , which is substantially higher than the $CA = 103^\circ$, measured on glass, covered by pure Rhodorsil. Embedding nanoparticles in the polymer matrix results in an increase of CA, which is more dramatic when the film is deposited on glass than on sandstone. At a concentration of approximately 1 % w/v, the film morphologies become saturated and the effect of the substrate roughness is diminishing.

10.3.5 *Effect of the Superhydrophobic Composite Films on the Aesthetic Appearance of Substrates*

In several applications, any effect on the aesthetic appearance of the substrate raised by the application of a protective coating is not acceptable. For example, water-repellent coatings designed to produce self-cleaning window glasses should be transparent in visible light [40]. Therefore, the polymer-nanoparticle composites, discussed herein, are not appropriate for glass protection because the white oxide nanoparticles clearly affect glass transparency. However, the effect of the suggested coatings on the aesthetic appearance of colored substrates can be within acceptable limits, especially when the color of the underlying substrate is close to the color coordinates of the white nanoparticles. This is demonstrated next.

Colorimetric measurements were first carried out on bare, untreated white marble, sandstone, and wood. The results for the L^* , a^* , and b^* coordinates are summarized in Table 10.3 and show that the three selected materials correspond to a broad range of the coloring palette, that is, from the bright white marble to the dark brown wood, with sandstone placed in between. Moreover, colorimetric measurements were carried out on the three aforementioned specimens covered by pure (hydrophobic) Silres BS 4004 and (superhydrophobic) Silres BS 4004-silica (7 nm and 2 % w/v) films. As described in Table 10.1, Silres BS 4004 is a waterborne siloxane product which makes it very attractive for practical applications, avoiding the use of volatile

Table 10.3 Results of colorimetric measurements, carried out on white marble, sandstone, and wood specimens which were (1) bare, untreated, and used as received, (2) covered by pure Silres BS 4004 films, and (3) covered by Silres BS 4004-silica composite films, prepared using silica particles (7 nm) at the concentration of 2 % w/v

Substrate	Color coordinates for untreated substrates			ΔE^* after film deposition	
	L^*	a^*	b^*	Pure Silres BS 4004	Silres BS 4004-silica composite
Marble	90.0	0.2	4.5	0.37	0.09
Sandstone	77.1	3.8	14.0	0.73	2.72
Wood	72.2	8.1	21.7	2.07	9.45

The surfaces of the films in (2) and (3) had hydrophobic and superhydrophobic properties, respectively

organic solvents. The global color differences (ΔE^*) occurring because of the film depositions were calculated as follows:

$$\Delta E^* = \sqrt{\Delta L^{*2} + \Delta a^{*2} + \Delta b^{*2}} \quad (10.3)$$

The calculated ΔE^* are summarized in Table 10.3. The use of nanoparticles to treat white marble had a positive effect on the aesthetic appearance of the specimen. When pure polymer was deposited, ΔE^* was 0.37. ΔE^* was reduced to 0.09 when the protective polymer film was blended with silica nanoparticles (composite film). Consequently, in the case of marble, the superhydrophobic composite coating induces less color change to marble than the pure hydrophobic polymer. This result is explained if it is considered that the white color of the silica nanoparticles is close to that of marble. In particular, the L^* , a^* , and b^* coordinates for the silica nanoparticles are 88.0, -2.5 , and -7.0 , respectively, which are close to the corresponding coordinates of white marble, reported in Table 10.3.

The use of silica nanoparticles had a negative effect on the aesthetic appearance of the brown sandstone. The application of the pure polymer on sandstone resulted in $\Delta E^*=0.73$ which increased to 2.72 when the polymer was enriched with silica nanoparticles. However, it is important to note that color changes corresponding to $\Delta E^*<3$ are typically not visible with naked eye. Consequently, the effect of the composite film on the aesthetic appearance of sandstone should be considered as being within the acceptable limit perceived by the human eye.

The color coordinates of silica, described above, are very different from the corresponding coordinates of the dark brown wood (Table 10.3). Consequently, the application of the composite film on wood resulted in a high ΔE^* (9.45) which is substantially higher than the $\Delta E^*=2.07$ (<3) result obtained when pure polymer was applied on wood. Therefore, silica nanoparticles had a major impact on the color of the wood specimen.

In summary, the results of Table 10.3 show that the method, described in the present report to impart superhydrophobicity to various substrates, is not necessarily accompanied by a severe penalty on the aesthetic appearance of the treated material. If the color coordinates of the substrate are comparable with the corresponding coordinates of the used nanoparticles, then the application of polymer-nanoparticle coatings can be acceptable from an aesthetic point of view, gaining simultaneously the beneficial superhydrophobic and water-repellent properties induced by these composite coatings.

10.4 Industrial Applications

Inspired by the hierarchical micro-/nanostructures found extensively in nature (e.g., lotus leaf, rose petal, mosquito eye, spider silks, butterfly wings, gecko feet, desert beetle, and water strider) [41], several strategies have been designed to produce surfaces of special wetting properties including superhydrophobicity and

water repellency which can be used in several applications such as self-cleaning coatings on outdoor surfaces (automobiles, buildings, etc.); anti-biofouling paints for boats; antisticking of snow for antennas, windows, and airplanes; microfluidics; lab-on-a-chip devices; metal refining; stain-resistant textiles; clotting preventive coatings in artificial blood vessels; and so on [41–43].

The method described in this article, where nanoparticles are embedded into polymers to achieve the desired hierarchical micro-/nanostructure, is a rapid, low cost method, which can be used to treat large surfaces, and can be implemented using various nanoparticles and polymers. Consequently, the method might be useful for some of the aforementioned applications of superhydrophobic coatings.

10.5 Conclusion

Various oxide nanoparticles (7–70 nm) were added in various polymer solutions, described in Table 10.1. Dispersions were sprayed on silicon. It was shown that the surfaces of the resulting composite polymer-nanoparticle films exhibit superhydrophobic and water-repellent properties (Figs. 10.2, 10.3, 10.4, and 10.5) which can be interpreted using the Cassie-Baxter model (Fig. 10.6), provided that an appropriate, elevated particle concentration was added in the polymer solution (Fig. 10.1). The extreme nonwetting properties are induced because the nanoparticles enhance the surface roughness at the micrometer and nanometer scale, as revealed by SEM images (e.g., Fig. 10.1). Furthermore, the spray method was applied to treat various substrates, achieving high and low contact angle and contact angle hysteresis, respectively, as shown in Figs. 10.7 and 10.8. Consequently, it is concluded that the simple suggested method for transforming the wetting properties of polymer films achieving extreme nonwetting is flexible, as it can be effectively applied to treat various substrates using common polymers and nanoparticles. Finally, it was shown that depending on the color of the underlying substrate, the superhydrophobic, water-repellent polymer-nanoparticle films may have negligible effect on the aesthetic appearance of the treated substrate.

References

1. Rozenberg BA, Tenne R (2008) *Prog Polym Sci* 33:40–112
2. Li S, Lin MM, Toprak MS, Kim DK, Muhammed M (2010) *Nano Rev* 1:5214. doi:[10.3402/nano.v1i0.5214](https://doi.org/10.3402/nano.v1i0.5214)
3. Hsieh C-T, Chen J-M, Kuo R-R, Lin T-S, Wu C-F (2005) *Appl Surf Sci* 240:318–326
4. Chibowski E, Hołysz L, Terpilowski K, Jurak M (2006) *Colloids Surf A* 291:181–190
5. Yüce MY, Demirel AL (2008) *Eur Phys J B* 64:493–497
6. Manoudis PN, Karapanagiotis I, Tsakalof A, Zuburtikudis I, Panayiotou C (2008) *Langmuir* 24:11225–11232
7. Ramaratnam K, Iyer SK, Kinnan MK, Chumanov G, Brown PJ, Luzinov I (2008) *J Engineered Fibers Fabric* 3:1–14

8. Cao L, Jones AK, Sikka VK, Wu J, Gao D (2009) *Langmuir* 25:12444–12448
9. Manca M, Cannavale A, De Marco L, Aricò AS, Cingolani R, Gigli G (2009) *Langmuir* 25:6357–6362
10. Manoudis PN, Karapanagiotis I, Tsakalof A, Zuburtikudis I, Kolinkeov B, Panayiotou C (2009) *Appl Phys A* 97:351–360
11. Du X, Li X, He J (2010) *ACS Appl Mater Interfaces* 2:2365–2372
12. Ke Q, Fu W, Wang S, Tang T, Zhang J (2010) *ACS Appl Mater Interfaces* 2:2393–2398
13. Tiwari MK, Bayer IS, Jursich GM, Schutzius TM, Megaridis CM (2010) *ACS Appl Mater Interfaces* 2:1114–1119
14. Karmouch R, Ross GG (2010) *Appl Surf Sci* 257:665–669
15. Gao N, Yan YY, Chen XY, Zheng XF (2010) *J Bionic Eng* 7:S59–S66
16. Ogihara H, Okagaki J, Saji T (2011) *Langmuir* 27:9069–9072
17. Men X, Zhang Z, Yang J, Zhu X, Wang K, Jiang W (2011) *New J Chem* 35:881–886
18. Ogihara H, Katayama T, Saji T (2011) *J Colloid Interface Sci* 362:560–566
19. Basu BJ, Kumar VD (2011) *ISRN Nanotechnol Article ID 803910*
20. de Ferri L, Lottici PP, Lorenzi A, Montenero A, Salvioli-Mariani E (2011) *J Cult Her* 12:356–363
21. Schutzius TM, Bayer IS, Jursich GM, Das A, Megaridis CM (2012) *Nanoscale* 4:5378–5385
22. Yilgor I, Bilgin S, Isik M, Yilgor E (2012) *Polymer* 53:1180–1188
23. Flores-Vivian I, Hejazi V, Kozhukhova MI, Nosonovsky M, Sobolev K (2013) *ACS Appl Mater Interfaces* 5:13284–13294
24. Li K, Zeng X, Li H, Lai X, Ye C, Xie H (2013) *Appl Surf Sci* 279:458–463
25. Lin J, Chen H, Fei T, Zhang J (2013) *Colloids Surf A* 421:51–62
26. Xue C-H, Ji P-T, Zhang P, Li Y-R, Jia S-T (2013) *Appl Surf Sci* 284:464–471
27. Seyedmehdi SA, Zhang H, Zhu J (2013) *J Appl Polym Sci* 128:4136–4140
28. Manoudis PN, Karapanagiotis I (2014) *Prog Org Coat* 77:331–338
29. D'Amato R, Caneve L, Giancristofaro C, Persia F, Pilloni L, Rinaldi A (2014) *J Nanoeng Nanosyst* 228:19–26
30. Barthlott W, Neinhuis C (1997) *Planta* 202:1–8
31. Feng L, Zhang Y, Xi J, Zhu Y, Wang N, Xia F, Jiang L (2008) *Langmuir* 24:4114–4119
32. Ebert D, Bhushan A (2012) *J Colloid Interface Sci* 384:182–188
33. Kulinich SA, Farzaneh M (2009) *Langmuir* 25:8854–8856
34. Johnson RE, Dettre RH (1964) *Adv Chem Ser* 43:112–135
35. Tserepi AD, Vlachopoulou M-E, Gogolides W (2006) *Nanotechnology* 17:3977–3983
36. Morra M, Occhiello E, Garbassi F (1989) *Langmuir* 5:872–876
37. Furmidge CGL (1962) *J Colloid Sci* 17:309–324
38. Cassie ABD, Baxter S (1944) *Trans Faraday Soc* 40:546–551
39. Karapanagiotis I, Manoudis PN, Savva A, Panayiotou C (2012) *Surf Interface Anal* 44:870–875
40. Karapanagiotis I, Manoudis PN, Zurba A, Lampakis D (2014) *Langmuir* 30:13235–13243
41. Lai Y-K, Chen Z, Lin C-J (2011) *J Nanoeng Nanomanuf* 1:18–34
42. Latthe SS, Gurav AB, Maruti CS, Vhatkar RS (2012) *J Surf Eng Mater Adv Technol* 2:76–94
43. Karapanagiotis I, Manoudis P (2012) *J Mech Behav Mater* 21:21–32